Immune cell trafficking from the brain maintains CNS immune tolerance

Mohammad G. Mohammad,[1] Vicky W.W. Tsai,[1] Marc J. Ruitenberg,[2] Masoud Hassanpour,[1]
Hui Li,[1] Prue H. Hart,[3] Samuel N. Breit,[1] Paul E. Sawchenko,[4] and David A. Brown[1]

[1]Laboratory of Neuroinflammation, St. Vincent's Centre for Applied Medical Research and University of New South Wales, Sydney, New South Wales, Australia.
[2]School of Biomedical Sciences and Queensland Brain Institute, University of Queensland, Brisbane, Queensland, Australia.
[3]Telethon Institute for Child Health Research, University of Western Australia, Perth, Western Australia, Australia.
[4]Laboratory of Neuronal Structure and Function, Salk Institute for Biological Studies, La Jolla, California, USA.

In the CNS, no pathway dedicated to immune surveillance has been characterized for preventing the anti-CNS immune responses that develop in autoimmune neuroinflammatory disease. Here, we identified a pathway for immune cells to traffic from the brain that is associated with the rostral migratory stream (RMS), which is a forebrain source of newly generated neurons. Evaluation of fluorescently labeled leukocyte migration in mice revealed that DCs travel via the RMS from the CNS to the cervical LNs (CxLNs), where they present antigen to T cells. Pharmacologic interruption of immune cell traffic with the mononuclear cell-sequestering drug fingolimod influenced anti-CNS T cell responses in the CxLNs and modulated experimental autoimmune encephalomyelitis (EAE) severity in a mouse model of multiple sclerosis (MS). Fingolimod treatment also induced EAE in a disease-resistant transgenic mouse strain by altering DC-mediated Treg functions in CxLNs and disrupting CNS immune tolerance. These data describe an immune cell pathway that originates in the CNS and is capable of dampening anti-CNS immune responses in the periphery. Furthermore, these data provide insight into how fingolimod treatment might exacerbate CNS neuroinflammation in some cases and suggest that focal therapeutic interventions, outside the CNS have the potential to selectively modify anti-CNS immunity.

Introduction

Since the work of Sheri and that of Murphy and Sturm (1), the prevailing paradigm has been that the inert immunological status of the CNS parenchyma is maintained by the exclusion of key components of the immune system. However, it is now known that systemic T lymphocytes, recruited by the choroid plexus (2), normally transit the CNS and participate in immune surveillance (3). Disease-promoting Th cells also directly penetrate the intact blood-brain barrier (4), and circulating APCs may also access the CNS parenchyma under normal conditions (5), mediating pathogenic T cell entry (6). The fact that the peripheral immune system has access to the CNS (7–9) in health and disease raises the question as to whether active mechanisms regulate CNS immune privilege. However, outside of established neuroendocrine pathways (10), a mechanism by which the brain can negatively regulate systemic immune responses directed against itself has not been defined. In other organs, APCs act in concert with draining LNs to promote or retard T cell activation, thus regulating organ-specific adaptive immune responses (11). A salient example of this concept is seen in the liver, which can regulate immunity against itself to the extent that MHC-mismatched transplants can be accepted without substantial immunosuppressive therapy (12). This occurs in part because of increased Treg function, which may be mediated by DCs found in the draining LNs (11, 12).

While mechanisms underlying immune surveillance in the normal CNS are not well understood, the role of the immune system in the CNS inflammatory disease MS and its animal model, EAE, have been studied extensively. These studies indicate that the cervical LNs (CxLNs) are a major site for systemic activation of CNS-specific T cells (13). The CxLNs receive input from the CNS in the form of antigens and perhaps DCs (14) and are a site for the activation of destructive anti-CNS immune responses (7–9, 14). However, there are also data to suggest the existence of immunoregulatory mechanisms that maintain and/or reestablish CNS integrity at this location (15). Animal studies indicate that autoreactive CNS T cells participate in maintaining CNS health (16, 17). Clinical data suggest that such autoreactive CNS T cells even participate in recovery from autoimmune neuroinflammatory diseases, such as MS (15). Interestingly, a recently licensed MS therapeutic, fingolimod (also known as FTY or FTY720), interrupts the trafficking of CNS-reactive T cells. This drug, a sphingosine-1-phosphate receptor (S1PR) inhibitor, prevents egress of lymphocytes from LNs (18). Fingolimod also prevents DC migration from peripheral organs to LNs (19, 20) and augments Treg function (21). While its dominant action is thought to be due to sequestration of autoreactive T cells in the LNs, it is possible that its other actions on non–T cell immune cell traffic are also consequential.

Here, using fingolimod treatment and a variety of other methods, we identified and characterized DC traffic from the CNS to the systemic immune compartment. This pathway directly modulated Treg function in the CxLNs and reduced CNS autoinflammatory disease, which suggests that it ultimately prevents pathogenic T cells from entering the CNS. Disrupting this pathway with localized infusion of fingolimod led to reduced CNS immune tolerance, enhanced anti-CNS autoimmune responses, and CNS inflammatory disease.

Results

CD11c$^+$ cells are associated with the rostral migratory stream (RMS). APCs are present in the choroid plexus and the meninges (22); however, their localization to the brain parenchyma in health is disputed

---

Authorship note: Mohammad G. Mohammad and Vicky W.W. Tsai contributed equally to this work.

Conflict of interest: The authors have declared that no conflict of interest exists.

Citation for this article: *J Clin Invest.* 2014;124(3):1228–1241. doi:10.1172/JCI71544.

(23, 24). Our examination of the normal mouse brain with dual immunolabeling demonstrated an association of CD11c$^+$ cells with the RMS, a pathway along which neuroblasts travel from the lateral ventricle to the olfactory bulb (OB) to replace olfactory interneurons (Figure 1A). CD11c$^+$ cells were found throughout the RMS (Figure 1B), including its terminal field, the granule cell layer of the OB. Additionally, these cells were found in the glomerular layer, adjacent to the cribriform plate. The distribution of CD11c$^+$ cells along the RMS and extending into the OB suggested that this might be an important area for CNS immunoregulation. We thus examined the RMS and surrounding white and gray matter structures for the presence of CD11c$^+$ cells. In the brains of normal, specific pathogen–free mice, CD11c$^+$ cells were preferentially associated with the RMS at significantly higher densities compared with surrounding white or gray matter structures (Figure 1C). To further characterize these putative DCs, we isolated CD11c$^+$ cells from 10 normal mice and examined them by fluorescence-activated cell sorting (FACS). They were predominantly CD11c$^+$CD11b$^+$ DCs, along with typical plasmacytoid DCs (pDCs) and a population of other DC phenotypes (Figure 1D and Supplemental Figure 2; supplemental material available online with this article; doi:10.1172/JCI71544DS1). To address the possibility that the specialized brain macrophage–like cells known as microglia might express CD11c, we performed further confocal examination of brain sections to define the anatomical location of the CD11c$^+$ cells and confirm that they were in fact DCs. This showed the presence of CD11c$^+$CD11b$^-$ cells in the choroid plexus and in association with the RMS (Figure 1, E and F); the lack of CD11b on these cells suggested they were true DCs. These cells and a subgroup of CD11c$^+$CD11b$^+$ cells had a similar appearance, distinctly different from that of resident CD11b$^+$CD11c$^-$ microglia (Figure 1F). Finally, we found that a substantial portion of these RMS DCs were truly located in the parenchyma (Figure 2).

CD11c$^+$ cells in the RMS are DCs derived from the circulation. To establish the origin of DCs present in the RMS, chimeric mice were generated by transplanting BM from syngeneic C57BL/6 mice expressing GFP under the control of the *Cx3cr1* promoter, which is active in monocyte lineage cells (25). 12 weeks after BM transplantation, GFP$^+$CD11b$^-$ cells were present along the course of the RMS and its terminal field. The parenchymal distribution of these cells was similar to that of normal, nonmanipulated mice, while the coexpression of GFP provided evidence of their peripheral (rather than CNS) origin. Using multilabel confocal microscopy, we identified subsets of GFP$^+$CD11b$^+$ and GFP$^+$CD11b$^-$ cells. These cells were again present in the choroid plexus adjacent to the origin of the RMS and throughout the entire RMS and its terminal field (Figure 3, A and B), which suggests the presence of both conventional (CD11c$^+$CD11b$^+$) and nonconventional (CD11c$^+$CD11b$^-$) DCs in this region. For macrophages, choroid plexus recruitment is mediated by VLA4 for attachment and CD73 for migration through the choroid epithelium (26). Indeed, systemic treatment of mice with the CD73 inhibitor methylene ADP led to significant changes in macrophage numbers, but not DC numbers (Supplemental Figure 1), which suggests that DC migration into the CNS is not modulated by CD73. Nonetheless, the presence of CD11c$^+$CD11b$^-$ cells with peripheral, circulatory origins represents strong evidence that true DCs are indeed present in the adult CNS.

DCs migrate from the CNS to the CxLNs. To determine whether leukocytes recruited to the CNS might migrate to the CxLNs, we infused CFSE, a vital fluorochrome that stably labels leukocytes, allowing their migration to be tracked. After 7 days of continuous intracerebroventricular (icv) infusion of CFSE into a lateral ventricle adjacent to the choroid plexus, CFSE-labeled immune cells were detected in the CxLNs (Figure 4A), but not in other secondary peripheral immune organs, including the inguinal LNs (Figure 4B) and spleen (data not shown). These findings indicate that CFSE-labeled cells accumulated in the CxLNs because of lymphatic-like drainage from the CNS.

If CFSE-labeled cells did transit from the brain, pharmacological interruption of this process should lead to their retention in the CNS. We therefore used fingolimod, which is known to alter lymphocyte and DC trafficking (19). We repeated the preceding experiment, but this time also gave mice daily i.p. injections of fingolimod or vehicle, starting prior to icv cannulation and continuing through the entire period of CFSE infusion. In vehicle-treated mice, CFSE-labeled leukocytes appeared in the CxLNs of mice sacrificed at the termination of CFSE infusion, and this accumulation was inhibited by systemic fingolimod treatment (Figure 4B). There was no significant accumulation of CD45$^+$ CFSE$^+$ events in the inguinal LNs (ILNs) of either fingolimod- or vehicle-treated mice (Figure 4B). We next characterized the composition of cells that were labeled with CFSE in the CNS and had migrated to the CxLNs. Perhaps not surprisingly, considering the injury induced by cannulation, the majority of cells that migrated to the CxLNs were CD11b$^+$, with forward and side scatter characteristics of macrophages. Consistent with the mediation of macrophage migration by S1P (27), fingolimod almost completely inhibited their transit to the CxLNs (Figure 4B). The next most abundant CFSE-labeled cell type found in the CxLNs was CD3$^-$CD11c$^+$ DCs, whose accumulation was also inhibited by fingolimod (Figure 4B). Virtually no CFSE$^+$CD3$^+$CD4$^+$ T cells were identified in CxLNs of CFSE-infused mice (data not shown). Consistent with this finding, systemic fingolimod treatment led to accumulation of these cell types in the CNS (Figure 4C). The absence of widespread CFSE staining in the CxLNs of mice treated with systemic fingolimod and the confinement of CFSE staining to specific leukocyte subsets also indicated that nonspecific leakage of dye to the CxLNs was not a confounding factor.

Systemic fingolimod treatment leads to DC accumulation in the normal CNS. Having established that fingolimod treatment virtually abolished egress of leukocytes from the brain, we next determined which leukocytes were preferentially retained in healthy brains. These experiments were performed in mice that had not experienced the injury that occurred due to CNS cannulation. Mice received daily systemic (i.p.) treatment of fingolimod or vehicle. Similar to mice undergoing icv cannulation, systemic fingolimod treatment of uncannulated mice led to significantly more DCs accumulating in the CNS (Figure 4C). To exclude the possibility that this was related to increased microglia activation for some unforeseen reason, we further quantified CD3$^-$CD11c$^+$CD11b$^-$ DCs, as these could not be classical microglia because of the absence of CD11b. We also found a significant increase in these cells with fingolimod treatment (Figure 4C). These findings indicate that DC entry and exit from the CNS are likely to be regulated by different mechanisms, as their egress (but not accumulation) was at least partly modulated by fingolimod. In the absence of cannulation, fingolimod treatment was not associated with significant differences in the accumulation of the CD45^{hi}CD11c$^-$CD11b$^+$ macrophage/polymorphonuclear cell (macrophage/PMN) subset (Figure 4C).

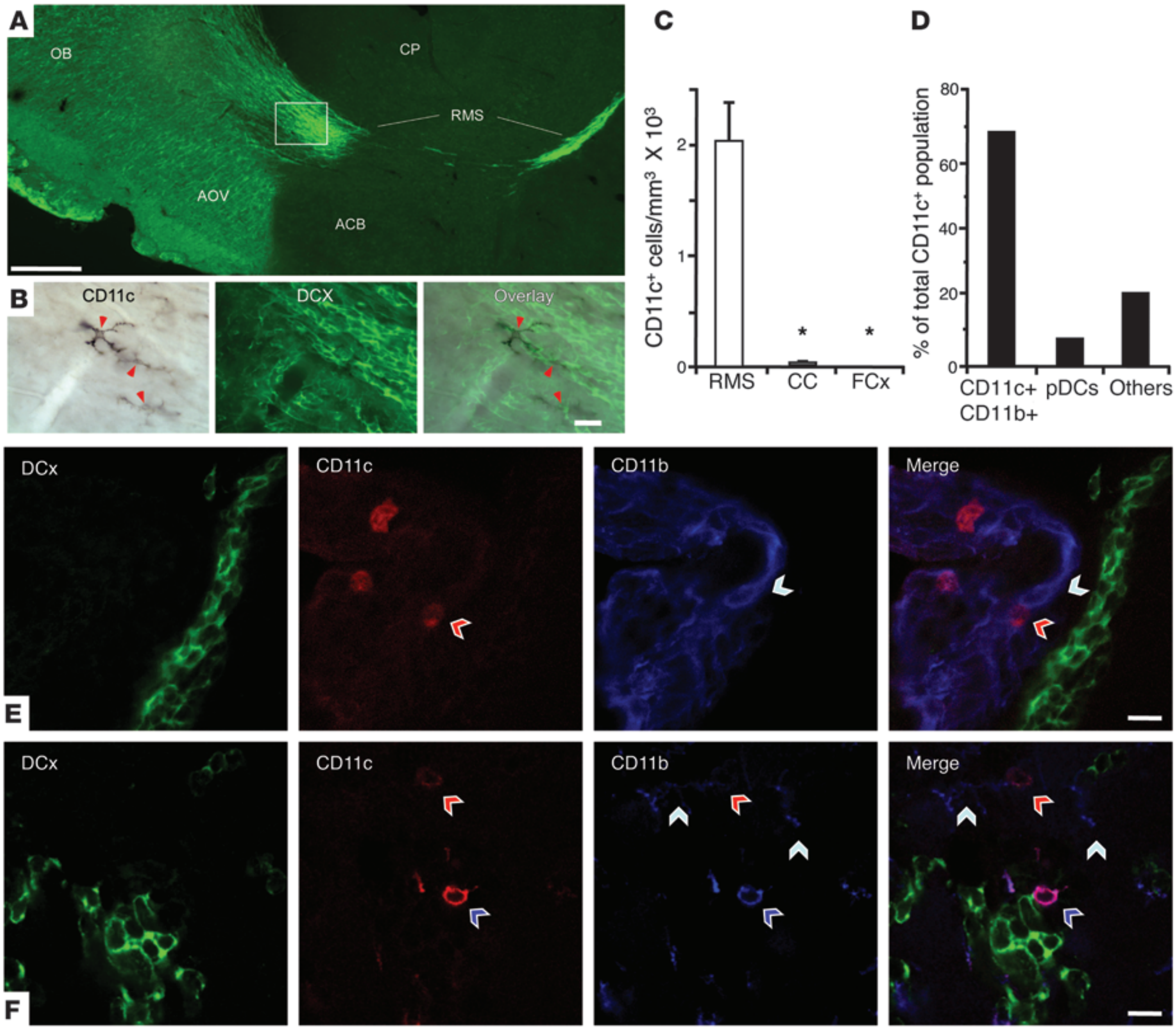

Figure 1
Immune cells are associated with the RMS. (**A**) Sagittal sections were labeled for CD11c by IHC, followed by IF staining for DCX (green), showing the course of the RMS from the subventricular zone to the OB. AOV, ventral anterior olfactory nucleus; ACB, nucleus accumbens; CP, caudate putamen. Box indicates the region shown at higher magnification in **B**. (**B**) The RMS, showing CD11c cells (red arrowheads) in close association with migrating DCX$^+$ neuroblasts. (**C**) CD11c$^+$ cells in the RMS were counted in at least 5 sections. The corpus callosum (CC) and frontal cortex (FCx) in the same sections were similarly examined. Data represent mean ± SEM. $^*P < 0.001$ vs. RMS. (**D**) Phenotypic analysis of CD11c$^+$ cells isolated from 10 mouse forebrains (for gating strategy, see Supplemental Figure 2). CD11c$^+$CD11b$^+$ cells represented 70% of DCs, pDCs represented 10%, and the remainder belonged to other CD11c$^+$CD11b$^-$ DC subsets (3 independent experiments). (**E**) IF confocal images for DCX (green), CD11b (blue), and CD11c (red). CD11c$^+$ (red arrowhead) and CD11b$^+$ (blue arrowhead) cells are identified in the choroid plexus adjacent to the DCX$^+$ subventricular zone in normal mice. (**F**) CD11c$^+$CD11b$^+$ DCs (blue arrow), CD11c$^+$CD11b$^-$ DCs (red arrow), and CD11b$^+$ microglia (white arrows) in close association with the RMS (green; DCX). Scale bars: 250 μm (**A**); 25 μm (**B**); 10 μm (**E** and **F**).

Systemic fingolimod treatment alters CD11c$^+$ cell distribution along the RMS. Our earlier experiments indicated that the majority of CD11c$^+$ cells, outside the normal CNS support structures, were associated with the RMS (Figure 1). Based on this finding, we reasoned that if egress of these cells was regulated by systemic fingolimod therapy, and if they traveled from the proximal to the distal RMS with migrating neuroblasts, fingolimod treatment should lead to their accumulation in the distal RMS. Furthermore, there should be no significant change in CD11c$^+$ cell numbers in the proximal RMS, as fingolimod therapy did not appear to affect their recruitment. Comparison of fingolimod- and vehicle-treated mice ($n = 6$ per group) revealed a significant difference in the distribution of CD11c$^+$ cells along the RMS. As predicted, CD11c$^+$ cells were at the same density in proximal parts of the RMS in both groups (Figure 5A). However, the density of CD11c$^+$ cells increased in the more distal parts of the RMS terminal field, peaking at the ventral glomerular layer of the OB, adjacent to the cribriform plate, after fingolimod treatment (Figure 5, A and B). These observations suggest that migration of CD11c$^+$ cells along the RMS was arrested at this point by fingolimod therapy. We next sought to determine whether DCs actually migrate along the RMS.

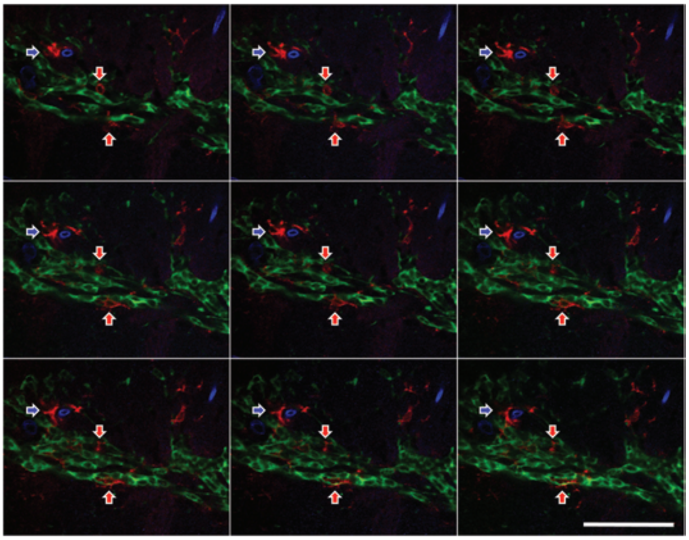

Figure 2

The majority of RMS CD11c⁺ cells are not associated with cerebral vasculature. To show that CD11c⁺ cells in the RMS were intraparenchymal, we performed serial optical sectioning (1-μm steps) through the RMS using confocal microscopy ($n = 5$). Sections were stained with DCX (RMS; green), CD11c (DCs; red) and CD31 (vascular endothelium; blue). Shown is a representative series demonstrating a typical perivascular CD11c⁺ cell (blue arrow) and 2 examples of the several CD11c⁺ cells in the RMS that were not associated with any vasculature (red arrows). Scale bar: 100 μm.

DCs migrate through the RMS. DCs were generated by culturing murine BM with fms-like tyrosine kinase 3 ligand (FLT3) (28), which yielded a highly enriched CD11c⁺ cell population (>95% purity) after 9 days in culture. These BM-derived DCs (BMDCs) were then labeled ex vivo with CFSE, after which 10^6 labeled cells were injected icv. Mice were killed 16 or 24 hours after injection ($n = 3$ per group). At 16 hours, CFSE⁺ BMDCs were observed in the proximal and middle RMS, as shown by staining for doublecortin (DCX; Figure 5C and ref. 29). By 24 hours, labeled cells had cleared the proximal and middle RMS and were seen in the terminal field of the RMS within the OB. To confirm that the RMS was unequivocally involved in DC migration from the proximal to the distal RMS, we ablated it with icv infusion of cytosine-β-D-arabinofuranoside (ARA-c) (30). In multiple experiments, this led to retention of DCs and macrophages in the brain (Figure 5E), similar to systemic fingolimod treatment of icv cannulated animals. Furthermore, direct quantification of DCs in the RMS showed that ablation of the subventricular zone and RMS did lead to failure of recruitment of DCs to the RMS (Figure 5D). As CXCL12 normally mediates neuroblast migration through the RMS (31), we treated mice systemically with AMD3100 to inhibit one of its receptors, CXCR4. This treatment resulted in an isolated increase in DCs in the mouse CNS (Supplemental Figure 3), similar to that observed with systemic fingolimod treatment (Figure 4C). Finally, we treated BMDCs ex vivo with fingolimod or vehicle and injected them icv as before, 48 hours after which the CxLNs were isolated. These showed that fingolimod directly acted on adoptively transferred DCs, reducing their egress from the CNS to the CxLNs (Figure 5, F and G). These data confirmed that DCs migrate through the RMS, possibly using chemotactic signals mediated by CXCR4. We next assessed the effect of perturbing this cellular pathway on CNS autoimmune inflammatory disease.

Fingolimod infusion to the RMS increases actively induced EAE severity. Systemic delivery of fingolimod inhibits EAE disease (32). Conversely, we discovered that targeting delivery of fingolimod to the RMS (Figure 6A) led to a dose-related *increase* in the severity of actively induced EAE with myelin oligodendrocyte glycoprotein$_{35-55}$ (MOG$_{35-55}$) peptide (Figure 6B). Infusions of the same dose of fingolimod — either icv into the lateral ventricle, at a CNS parenchymal site distant from the RMS (hippocampus), or systemically — led to relative reductions in clinical EAE (Figure 6, C and D). Together, these data suggested that modulation of immune cell traffic through the RMS leads to altered CNS immunoregulation. As fingolimod treatment of the RMS led to deviation of regulatory immune responses and enhanced anti-CNS immunity, we next investigated whether targeted delivery of this drug could induce spontaneous EAE.

Fingolimod infusion to the RMS increases spontaneous EAE incidence. While the majority of Th cells of Vβ11 T cell receptor transgenic 2D2 C57BL/6 mice respond to MOG, they display a low rate of spontaneous CNS-wide disease. Whereas up to 30% of 2D2 mice develop optic neuritis over a 3-month period, only about 6% go on to develop spontaneous classical (rather than opticospinal) EAE (33, 34). Breaking immune tolerance in 2D2 mice (with pertussis toxin treatment alone) significantly enhances EAE incidence to about 60%, whereas MOG vaccination (without pertussis toxin treatment) does not induce EAE (34). As one of pertussis toxin's principal actions is to modify immune cell migration (35), we hypothesized that immune cells associated with the RMS may restrain systemic anti-CNS immune responses in 2D2 mice. To test this contention, we administered fingolimod or vehicle directly targeting the RMS (referred to herein as RMS-fingolimod and RMS-vehicle treatment, respectively). Separate cohorts received fingolimod or vehicle via RMS and icv infusion, or directly to the CxLNs via s.c. lymphatics (36), the latter bypassing the CNS. RMS-fingolimod led to a 63% incidence of classical EAE (10 of 16 mice) compared with RMS-vehicle control mice (0 of 9; $P < 0.001$). Furthermore, there was no case of EAE in mice that had fingolimod or vehicle infused to the lateral ventricle ($n = 4$) or to the CxLNs ($n = 11$). Among the 10 mice that developed symptoms of EAE, clinical scores ranged from 1 to 5 (mean ± SEM, 2.0 ± 0.4; Figure 7A). These data confirmed the unique capacity of RMS-fingolimod delivery to induce EAE in this otherwise-resistant mouse line.

We also quantified CNS-specific Vβ11⁺ T cells in the spinal cord of 2D2 mice that received RMS-targeted treatment; this area is affected in classical EAE, but distant from the infusion site. FACS analysis of spinal cord mononuclear cells revealed that the absolute number and proportion of Vβ11⁺ T cells

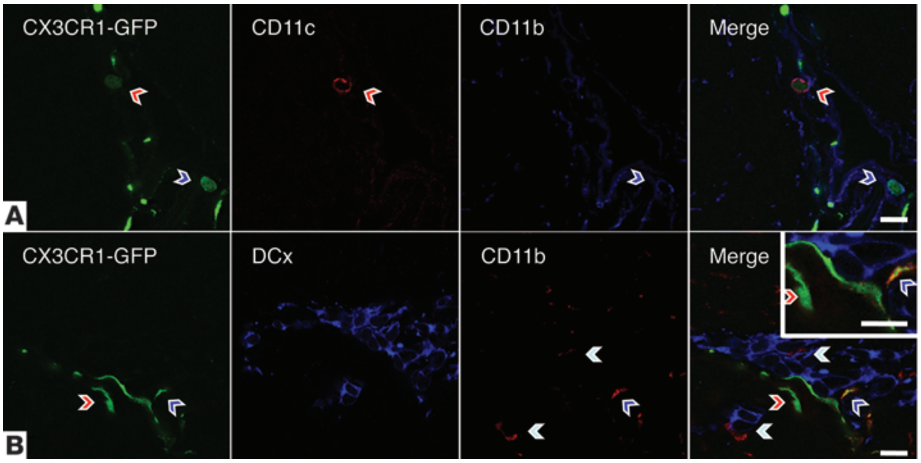

Figure 3
Blood-derived DCs are recruited to the RMS. *Cx3cr1*$^{+/gfp}$-to-WT BM chimeric mice were killed 12 weeks after BMT. Brain sections were labeled for DCX (blue), CD11b (blue or red), and/or CD11c (red); GFP fluorescence is shown in green. (**A**) Confocal images showing the presence of both GFP$^+$CD11c$^+$ cells (red arrow) and GFP$^+$CD11b$^+$ cells (blue arrow; i.e., derived from donor BM) in the choroid plexus. (**B**) GFP$^+$CD11b$^-$ circulation-derived cells, presumably nonmacrophage/microglia and therefore DCs, were again seen in close association with the RMS (red arrow), alongside GFP$^-$CD11b$^+$ (white arrows) and GFP$^+$CD11b$^+$ cells. Scale bars: 10 μm.

was significantly higher in fingolimod- versus vehicle-infused mice (Figure 7B and Supplemental Figure 5B), consistent with increased neuroinflammation.

Treg function is compromised in the CxLNs of RMS-fingolimod–treated mice. CxLNs were harvested from untreated 2D2 mice or those subjected to RMS-fingolimod or RMS-vehicle treatment. To identify Tregs, we stained CxLN cells from untreated mice with CD3, CD4, CD25, CD127, and FoxP3. This showed that most, if not all, CD25$^+$CD127^{lo} cells expressed FoxP3 (Supplemental Figure 6), identifying them as bone fide inducible Tregs. We then determined the proportion of antigen-specific T effector cells (Teffs) and Tregs in the CxLNs of treated 2D2 mice. We stained cells with anti-CD45, -CD3, -CD4, -CD44, -CD62L, -CD25, and -CD127 in addition to a Vβ11 antibody to identify the transgenic MOG-specific T cells (Supplemental Figure 7). While the proportion of CxLN CD25^{hi}CD127^{lo} Tregs was not significantly different between mice treated with vehicle or fingolimod (Figure 7D), the Vβ11$^+$ Treg/Teff ratio in the CxLNs was significantly and inversely related to the proportion of CNS-specific cells in the spinal cord ($P = 0.002$; Figure 7C and Supplemental Figure 7), the latter being a quantitative measure of EAE disease severity. As antigen-specific T cells are activated in the CxLNs prior to migrating to the CNS (14), and Tregs modulate this activation (37), we hypothesized that RMS-fingolimod treatment causes a deficit in Treg function in the CxLNs, thus enhancing anti-CNS immune responses.

RMS-fingolimod administration breaks CNS immune tolerance. To determine whether CxLN Treg function was compromised after RMS-fingolimod infusion of treated 2D2 mice, we directly compared the effect of Treg depletion on in vitro antigen-specific CxLN T cell activation. Treg depletion was accomplished by either leaving or removing CD25^{hi} cells from the mononuclear cell preparation derived from CxLNs (Supplemental Figure 8). This approach was designed to measure the functional capacity of DC-inducible CD25^{hi}CD127^{lo} Tregs (reviewed in ref. 38). While we recognize that this approach also removes CD25$^+$ Teffs, the removal of these cells biases against increased T cell activation. Nonetheless, to exclude any unequal bias, we quantified the antigen-specific Teff frequency in the CxLNs after RMS-fingolimod or RMS-vehicle treatment, as well as after similar treatments administered directly to the CxLNs, and found no significant differences (Figure 7, E and F). RMS-fingolimod treatment resulted in significantly less restraint of Teff cell activation compared with RMS-vehicle, as indicated by a smaller increase in antigen-specific activation with and without CxLN Tregs ($P = 0.02$; Figure 7G). Given that the CxLNs of the RMS-fingolimod and RMS-vehicle groups showed equal numbers of Tregs (Figure 7D), these data suggest that CxLN Tregs after RMS-fingolimod treatment are less efficient at suppressing T cell activation. In direct contrast, there were no significant differences in the activity of ILN Tregs, regardless of treatment (Figure 7G). As DCs rather than T cells were prevented from traveling to the CxLNs from the CNS, we postulated that DCs mediated the changes in Treg function in the CxLNs.

DCs modify anti-CNS immunity in the CxLNs via regulation of Treg activity. To determine whether impaired DC traffic from the brain, as a result of targeted fingolimod treatment, mediates the altered Treg activity in the CxLNs, we used a model of delayed-type hypersensitivity (DTH). This model is capable of determining whether DCs modify antigen-specific Teff responses in the CxLNs in vivo (39), and whether CxLN Treg activity is similarly modified. In this case, we examined whether RMS-fingolimod treatment altered the capacity of CxLN DCs to modulate Th cell responses to MOG peptide. WT C57BL/6 mice were subjected to a 4-week RMS-fingolimod or RMS-vehicle infusion, after which CxLNs were harvested, mononuclear cells were isolated and surface labeled, and CD45$^+$CD3$^-$CD11$^+$ DCs were purified by FACS to greater than 99% purity (Supplemental Figure 10). The DCs from a single mouse ($4–8 \times 10^4$ cells) were injected into a pinna of a separate C57BL/6 mouse, which had received a single s.c. vaccination with MOG peptide in complete Freund's adjuvant 7 days earlier. As a control, the other ear of the same mouse was injected with the acellular vehicle. 10 days later, both ears were challenged with MOG peptide by directly injecting it into the subcutis. To assess T cell–mediated antigen recall responses, ear swelling was measured 24 hours after challenge (39), with increasing ear swelling indicating a greater response. The swelling in the control ear that received the acellular vehicle injection was considered to represent the immune recall response, wholly attributable to the MOG vaccination. The swelling of the ear injected with DCs was directly compared with the control ear of the same mouse and expressed as a percentage of the control ear swelling. In replicate experiments, DCs isolated from the CxLNs of mice with RMS-fingolimod treatment mediated a significant increase in recall responses to the CNS antigen MOG, confirming enhanced anti-CNS immune responses in the CxLNs, whereas RMS-vehicle controls showed no such change (Figure 8A).

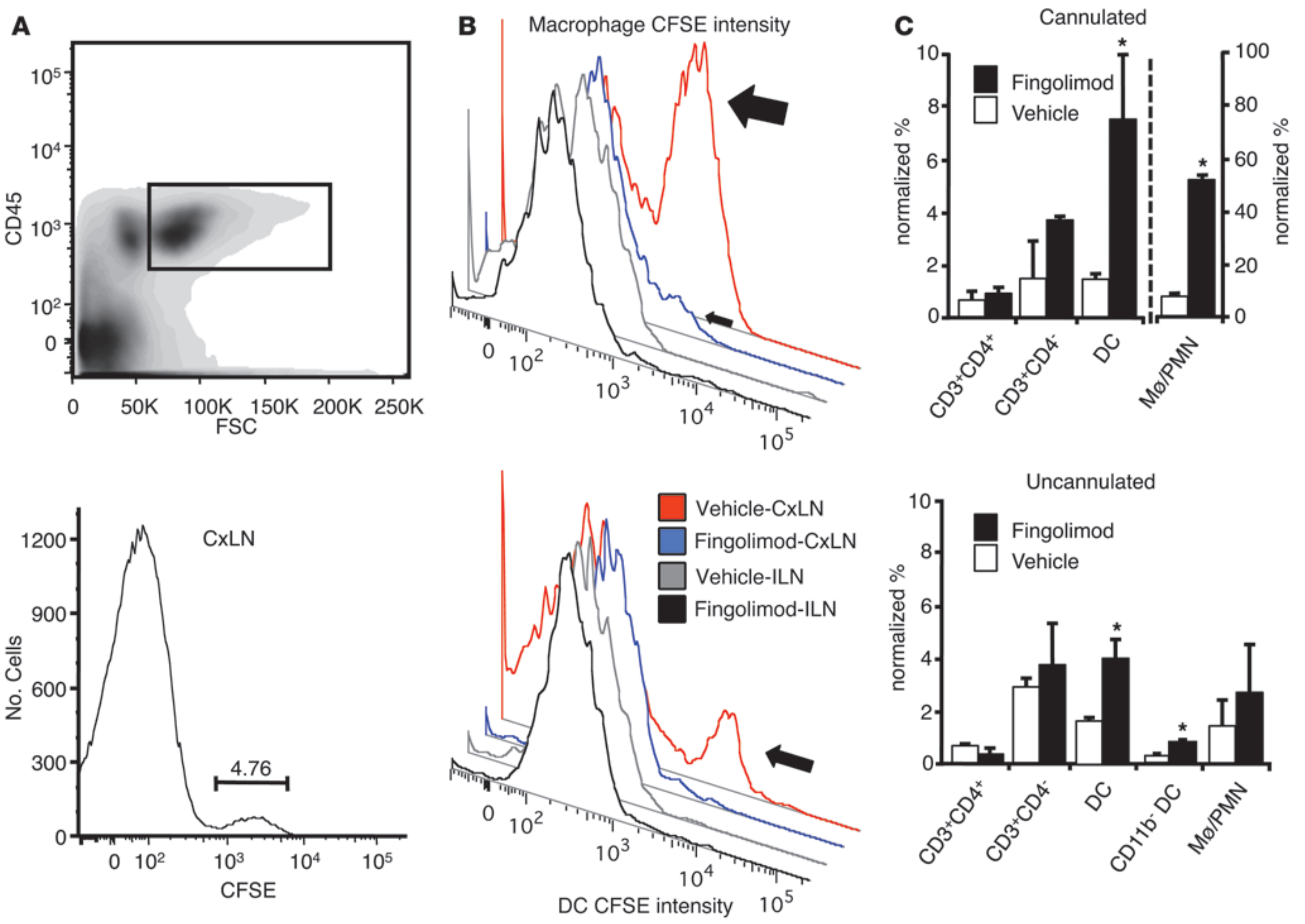

Figure 4

Leukocytes migrate from the CNS to CxLNs. In icv-cannulated mice, after 7 days of CFSE infusion, CxLN CD45$^+$ cells were gated and examined for CFSE labeling. (**A**) CFSE-labeled cells were discerned in all mice. The percentage of CFSE$^+$ cells is indicated. (**B**) The same experiment repeated with fingolimod or vehicle administered i.p. ($n = 6$; 3 independent experiments), beginning 1 day prior to icv cannula implantation. For gating of CFSE$^+$ CxLN and ILN monocytes, see Supplemental Figure 4. Top: Vehicle-treated mice (large arrow) had substantial populations of CFSE$^+$ presumed macrophages (CD45$^+$CD3$^-$B220$^-$CD11c$^-$CD11b$^+$), which were significantly reduced in CxLNs from fingolimod-treated mice (small arrow) and absent in ILNs of either vehicle- or drug- treated mice. Bottom: CFSE$^+$ DCs (CD45$^+$CD3$^-$CD11c$^+$) were only seen in CxLNs of vehicle-treated mice (arrow), and their accumulation was completely inhibited by systemic fingolimod treatment. (**C**) Mice that had CFSE infused by icv cannula had their brains removed, and mononuclear cells were extracted for FACS. Top: DC and macrophage/PMN accumulation in the brains of cannulated mice. Bottom: To determine which cell type(s) may have accumulated as a result of injury associated with icv cannulation, we also administered fingolimod (6 μg/d) or vehicle ($n = 6$; 3 independent experiments) i.p. to noncannulated mice, which demonstrated an increased frequency of DCs in the CNS as assessed by FACS ($P = 0.018$), with no differences in corresponding macrophage/PMN or T cell numbers. Data represent mean ± SEM. $^*P < 0.05$.

DCs isolated from the CxLNs of mice receiving icv vehicle or fingolimod showed no capacity to regulate the Teff response to MOG in the CxLNs, as indicated by similar degrees of swelling in acellular vehicle– and DC-injected ears (Figure 8A). These data suggested that impaired egress of DCs from the CNS as a result of RMS-fingolimod treatment was responsible for increased CNS antigen recall responses in the CxLNs. However, a direct effect of fingolimod on CxLN DCs cannot be excluded.

Fingolimod does not alter the inflammatory activity of CNS DCs. To test whether direct effects of fingolimod on DC inflammatory, rather than migratory, capacity were responsible for our results, we took advantage of the pharmacokinetic properties of fingolimod, which leads to preferential CNS concentration after systemic therapy (32). This ensured that any DCs isolated from the CNS would be exposed to fingolimod in vivo. In this case, DCs from the CxLNs could not be used, as we had shown that systemic fingolimod treatment was likely to alter traffic to the CxLNs and thus bias our results. We treated groups of 10 mice with vehicle or fingolimod (6 μg/d i.p.) for 7 days. CNS DCs were isolated, as above, from the forebrain with the meninges removed (Supplemental Figures 2 and 10). We then compared their capacity to modulate CNS antigen recall responses using the DTH model. There were no significant differences in the recall responses when DCs were isolated from vehicle- or fingolimod-treated mice and subsequently delivered to the CxLNs (Figure 8B), which suggests that the direct effects of fingolimod on DCs did not alter their capacity to modulate inflammation. Having discounted a direct effect of fingolimod on DCs, and considering our observation of

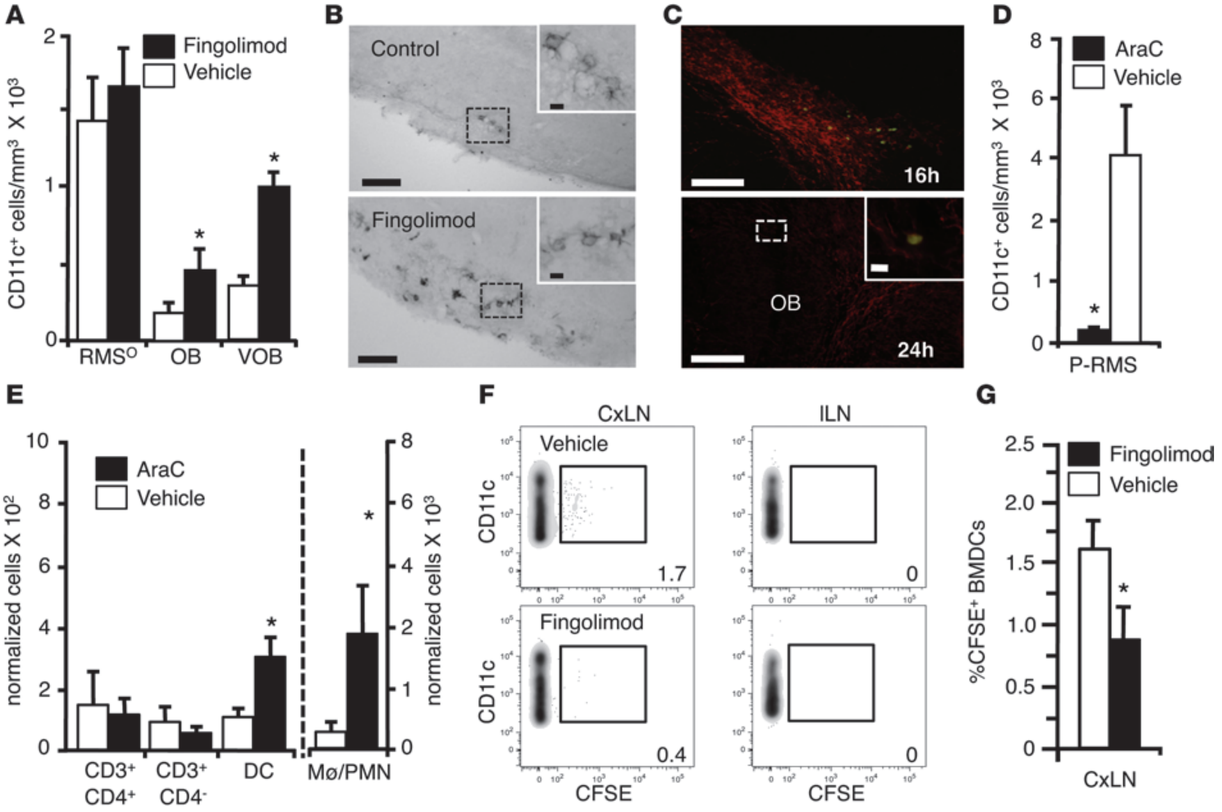

Figure 5

CD11c^{+} cells are recruited to the proximal RMS and travel to the OB, and RMS disruptions leads to their accumulation. (**A**) With i.p. fingolimod treatment ($n = 5$), the frequency of CD11c^{+} cells in the proximal RMS (RMS^{O}) remained unchanged. However, the CD11c^{+} cell density significantly increased in the terminal field of the RMS ($P = 0.042$) and was further enriched in the ventral part of the OB (VOB; $P = 0.014$). (**B**) Representative sections of the ventral OB showing accumulated CD11c^{+} cells in fingolimod-treated mice compared with vehicle controls. (**C**) CFSE-labeled BMDCs were given icv ($n = 3$/group). CFSE^{+} cells (green) were present in the proximal-mid RMS (DCX, red) at 16 hours (top), and by 24 hours (bottom) had reached the OB. (**D**) The RMS was ablated with a 7-day icv ARA-c infusion. There were significantly fewer CD11c^{+} DCs in the proximal region of the ablated RMS ($P = 0.04$, $n = 3$/group). (**E**) However, in similarly treated mice, FACS analysis of CNS mononuclear cells from the forebrain showed significantly increased macrophages and DCs, similar to systemic fingolimod treatment ($P = 0.03$, $n = 6$; 2 independent experiments). (**F**) Representative FACS plots showing CFSE-labeled DCs that had migrated from CNS to CxLNs isolated 48 hours from mice after 3 icv injections of fingolimod-pretreated (100 nM for 24 hours), CFSE-labeled BMDCs (1 × 10^{6} cells/injection) at 12-hour intervals ($n = 7$/group, 2 independent experiments). (**G**) Fingolimod treatment of DCs significantly reduced their migration into CxLNs ($P = 0.042$, $n = 7$; 2 independent experiments). Scale bars: 100 μm; 10 μm (insets). Data represent mean ± SEM. *$P < 0.05$.

altered Treg function in the CxLNs as a result of RMS-fingolimod treatment, we next examined whether adoptively transferred DCs directly modulate Treg function in the CxLNs.

DCs directly modulate Treg function in the CxLNs. To ascertain that transferred DCs modulate anti-CNS immunity by regulating CxLN Treg activity, we examined mice that had CxLN DCs transferred to the ear. After MOG challenge (Figure 8A), the DC- and vehicle-injected ears had their draining CxLNs isolated separately, after which Treg activity was determined, as we had done before (Figure 7G). Treg activity was significantly lower in CxLNs that received DCs from RMS-fingolimod compared with RMS-vehicle–treated mice (Figure 8C). These data thus support the contention that fingolimod restrains the egress of DCs from the brain that would otherwise enhance Treg activity. Furthermore, they indicate that there must be a subpopulation of DCs in the normal CNS that restrain anti-CNS immune responses in the CxLNs.

A subset of forebrain DCs restrains anti-CNS immunity. Our preceding data suggested the presence of a subset of CNS DCs that suppresses anti-CNS immune responses in the CxLNs. We therefore isolated the DCs from the forebrain, where DCs are concentrated along the RMS (Figures 1–3), carefully denuded of meninges to remove any associated DCs. The remaining, predominantly RMS-associated DCs of 10 normal mice were purified by FACS (Supplemental Figure 10). We then tested the ability of sorted CD45^{hi}CD3^{-}CD11c^{+}CD11b^{+} and CD45^{hi}CD3^{-}CD11c^{+}CD11b^{-} CNS DCs to modulate anti-CNS responses in our DTH model. Isolated DCs were directly injected into one ear, and acellular vehicle control into the other, of MOG-vaccinated mice, and recall responses to MOG were measured. Only CD45^{hi}CD3^{-}CD11c^{+}CD11b^{-} CNS DCs were capable of significantly reducing antigen recall responses to MOG (Figure 8D). This DC subpopulation includes pDCs that are known to augment Treg responses (40). These data confirmed that the normal mouse CNS contains a CD45^{hi}CD3^{-}CD11c^{+}CD11b^{-} cell population capable of suppressing anti-CNS responses in the CxLNs. To show that this effect was likely antigen specific, we performed the same experiment but substituted methylated BSA for MOG for vaccination and chal-

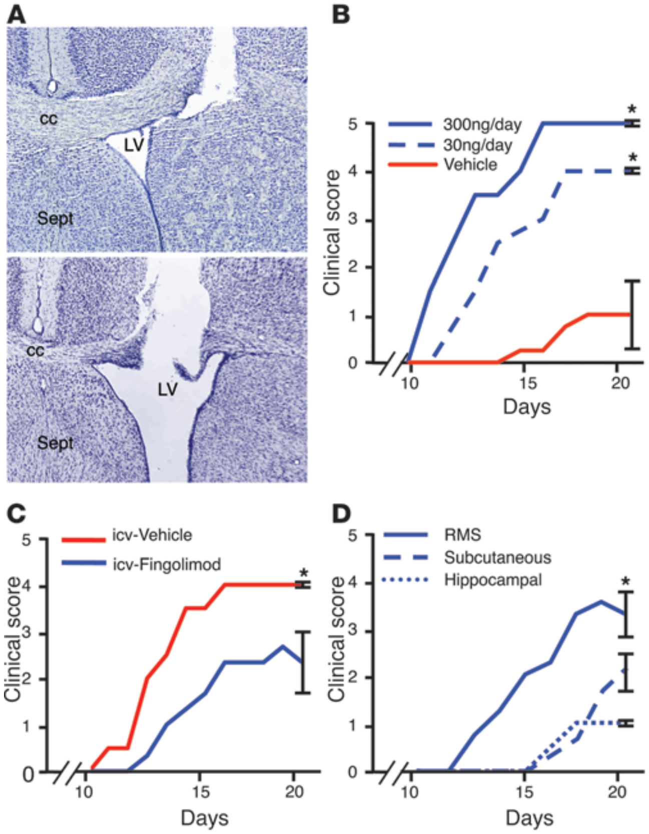

Figure 6

Targeted RMS-fingolimod treatment increases MOG-induced EAE severity. (**A**) RMS-fingolimod treatment. Cannulae were implanted near the origin of the RMS (top), in the lateral ventricle (LV; bottom), or the hippocampal formation (not shown). Fingolimod was delivered over a 4-week period via an osmotic minipump. Sept, septum. (**B**) RMS-fingolimod treatment beginning 1 week prior to EAE induction led to a dose-dependent increase in disease severity ($n = 3$/group), with mice receiving 300 ng/d all dying by day 15. Animals receiving 30 ng/d were less severely affected, but reliably more so than vehicle-infused controls ($P < 0.001$). (**C**) Mice that received icv fingolimod (300 ng/d; $n = 3$) developed significantly less severe EAE than vehicle controls ($P = 0.004$). (**D**) Infusion of fingolimod to the hippocampus or systemically also resulted in milder clinical disease compared with RMS-fingolimod treatment ($n = 3$ per group; $P < 0.001$). $^*P < 0.05$.

lenge, and found no significant modulation of DTH (Figure 8E). This observation suggests that DCs modulate CxLN responses in a CNS antigen–specific manner.

Discussion

Many studies have demonstrated the tolerogenic properties of the CNS parenchyma. Such findings, combined with the identification of CNS anatomical barriers, suggested that cellular immune components have limited access to the CNS (2). However, these observations are not consistent with the now widely accepted observation that T cells are present in the normal CNS. While previously controversial (5, 23, 24, 41), our present findings clearly indicate that circulation-derived CD11c$^+$ DCs can also access selected regions of the healthy CNS parenchyma, as they do in other solid tissues. Here, we identified a novel physiological pathway of DC traffic from the CNS to the CxLNs that actively downregulated CNS autoimmunity in the peripheral immune compartment. We further showed that this pathway of DC migration was anatomically and functionally associated with the RMS and amenable to therapeutic intervention.

The most pertinent question arising from these data is how the presence of DCs in the parenchyma might have previously passed unnoticed. This is likely because of the common practice of generating coronal sections for most purposes. In this orientation, the RMS occupies a very small proportion of the entire section. As the density of DCs is relatively sparse, these cells would be easily missed in this plane of sectioning. Sagittal sections, on the other hand, display the entire course of the RMS, more readily allowing for the identification of any DCs contained within it. Using this approach, we showed that DCs, having gained access to the lateral ventricle, migrated along the path of the RMS (Figure 5C). The origin of RMS-associated DCs in the unmanipulated CNS was not definitively identified in this study, although our data suggested that they originate from the circulation (Figure 3) and likely enter via the choroid plexus, largely independent of mechanisms that were recently reported to regulate macrophage recruitment at this site (26). However, they might also arise from a recently described CNS-resident precursor population (5). Regardless of their possible point(s) of entry, our findings clearly indicated that once recruited to the RMS, they migrate to the distal OB and then to the CxLNs (Figures 4 and 5), probably by accessing the nasal mucosal lymphatics (Figure 9 and refs. 42–44). There, they interact with T cells and regulate Treg activity, which in turn regulates CNS-specific Teff activation. Specific interruption of this pathway in the brain with fingolimod prevented DCs from reaching the CxLNs. This had the effect of breaking CNS immune tolerance, leading to neuroinflammatory disease.

In experiments where there was cannula insertion into the CNS, systemic fingolimod treatment prevented both macrophages and DCs from leaving the CNS (Figure 4). It seems likely that this macrophage accumulation occurred as a consequence of cannula insertion, which inevitably causes some brain injury. In the noninjured CNS, systemic fingolimod and AMD3100 treatment resulted in accumulation of DCs alone, apparently because they were prevented from leaving the CNS (Figure 4C). Interestingly, ablation of the RMS with ARA-c also impeded cell egress from the CNS, perhaps identifying a role for immune cell trafficking along the RMS in the resolution of CNS inflammation. The accumulation of inflammatory cells and the prevention of their egress in the continued inflammation associated with active MS plaques may provide an explanation for the increasing numbers of adverse events associated with fingolimod treatment in MS (45). However, the identity of the inflammatory cell(s) that might be detrimental in this context is not clear. It may be speculated that these are macrophages associated with ongoing injury in MS plaques.

The association of APCs, like DCs, with a neurogenic pathway like the RMS may seem surprising, although it should be noted that the RMS is organized around the wall of the olfactory ventricle (or remnants thereof). These DCs would be expected to participate in CNS immunoregulatory activities, as occurs in other solid organs, by migrating to draining LNs and regulating immune cells such as Tregs (11). However, we should note that we have not examined the Virchow-Robin spaces, which also harbor DC–T cell interactions (46). In any case, similar to other solid organs, our data strongly suggest that suppression of anti-CNS

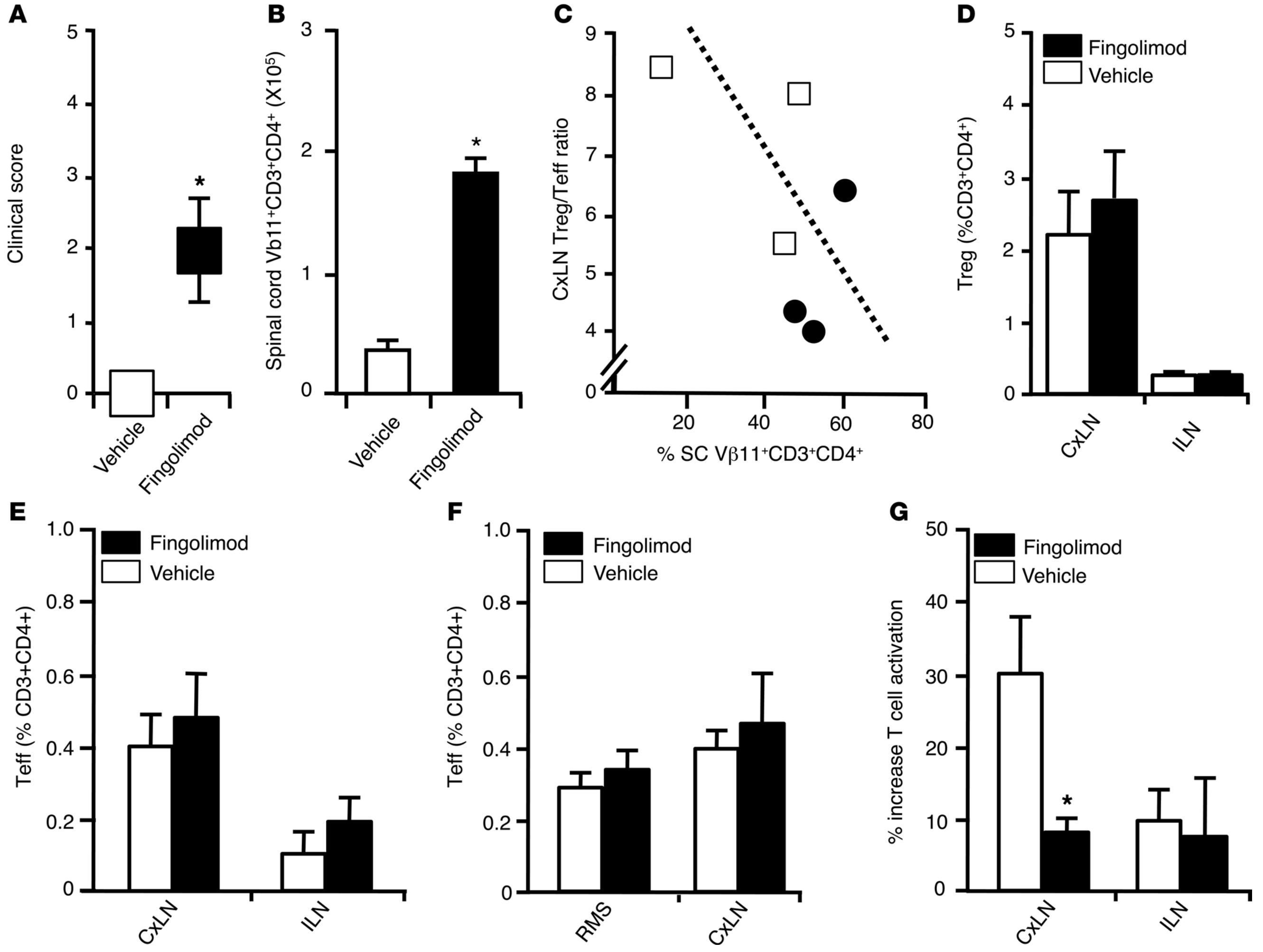

Figure 7

RMS-fingolimod treatment induces EAE by disrupting CxLN Treg function. (**A**) EAE incidence in 2D2 mice increased from 0% with RMS-vehicle treatment (n = 9) to 63% (10 of 16; 4 independent experiments) with RMS-fingolimod treatment. (**B**) These mice also had more antigen-specific T cells in spinal cords ($1.7 \pm 0.1 \times 10^5$ vs. $0.4 \pm 0.2 \times 10^5$; $P = 0.03$; 3 independent experiments), and (**C**) the Treg/Teff ratio in the CxLNs was negatively related to antigen-specific T cells in spinal cord (SC; n = 6; $P = 0.002$; 3 independent experiments; see also Supplemental Figures 6 and 7). (**D** and **E**) They also had no differences in (**D**) the number of antigen-specific Tregs between CxLNs and ILNs (CxLN, $P = 0.9$; ILN, $P = 0.5$) or in (**E**) the proportion of antigen-specific Teffs as a percentage of total T cells (CxLN, $P = 0.6$; ILN, $P = 0.3$). (**F**) RMS-fingolimod or direct CxLN fingolimod treatment did not affect the proportion of Teffs ($P = 0.6$; n = 6; 2 independent experiments). (**G**) Separate RMS-fingolimod– or RMS-vehicle–treated 2D2 mice (n = 9; 3 independent experiments) had their Treg activity assessed in their CxLNs (see Methods and Supplemental Figures 8 and 9). There was a significant increase in antigen-specific T cell activation when $CD25^{hi}$ Tregs were removed from the CxLN mononuclear population ($P = 0.023$) of RMS-vehicle–treated, but not RMS-fingolimod–treated, CxLN isolates, in contrast to ILNs (n = 18; 3 independent experiments), indicative of reduced Treg activity in the CxLNs of RMS-fingolimod–treated mice. Data represent mean ± SEM. $^*P < 0.05$.

responses in the CxLNs is mediated by DCs that have traveled from the CNS. Further support for this assertion was our finding that DCs — alone, traveling to the CxLNs — mediated changes in the immune response to CNS antigens. We demonstrated this by showing reduced CNS immune responses in a recipient mouse's CxLN after receiving $CD11c^+CD11b^-$ DCs isolated from the CNS of a normal mouse (Figure 8D).

Recent work has identified the CxLNs as a major site of activation of anti-CNS immune responses in MS (13, 47). Antigens delivered to the CNS drain to the CxLNs, where they are processed by DCs (7). DCs injected into the brain parenchyma also migrate to CxLNs (14). CNS-specific T lymphocytes are then activated in the CxLNs prior to their migration to the CNS (14). Preventing DC migration to the CxLNs through targeted RMS-fingolimod treatment resulted in impaired Treg function, which substantially increased the incidence of spontaneous EAE in otherwise resistant 2D2 mice. EAE incidence in 2D2 mice (Figure 7A) was similar to that observed with pertussis toxin treatment, which is also known to inhibit immune cell migration (34). The lack of EAE induction when fingolimod was delivered directly to the CxLNs via s.c. lymphatics indicates that a direct effect of fingolimod on the CxLNs is unlikely. Furthermore, broad targeting of meningeal inflammatory cells, other similar parenchymal CNS cells, or the whole CNS (32) by icv, hippocampal, or systemic fingolimod delivery, respec-

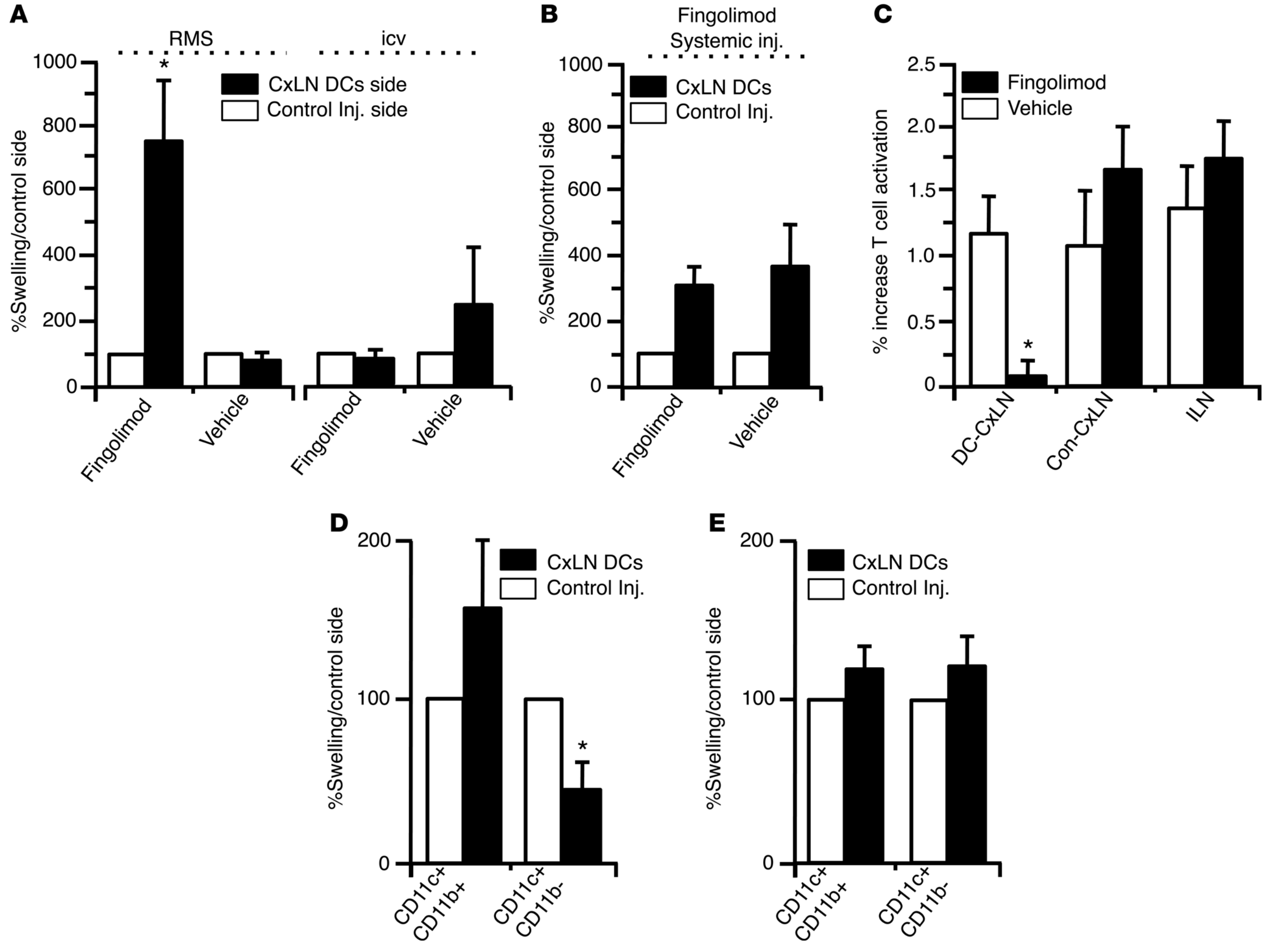

Figure 8

CNS-derived DCs modulate anti-CNS immunity in the CxLNs. (**A**) CxLN DCs were purified from C57BL/6 mice treated with RMS-fingolimod or -vehicle, or icv fingolimod or vehicle, for 4 weeks. These or acellular vehicle were injected into each pinna of separate C57BL/6 mice prior to MOG DTH assessment (see Methods). Only DCs from fingolimod-treated mice increased MOG DTH responses (RMS-fingolimod, $n = 12$/group; icv fingolimod, $n = 6$/group; $P = 0.003$; 3 independent experiments). (**B**) Separate C57BL/6 mice were treated with fingolimod or vehicle i.p. for 14 days ($n = 10$; 3 independent experiments), and CNS DCs were FACS purified and tested in the DTH model, which showed they similarly modified DTH and were not altered by direct fingolimod exposure. (**C**) 10 mice (5 vehicle; 5 fingolimod) were randomly selected from **A**, and CxLNs draining the vehicle control– or DC-treated ears were isolated separately for Treg functional assessment. Only the CxLNs draining ears that had RMS-fingolimod DCs delivered had significantly reduced Treg activity ($n = 5$; $P = 0.01$). (**D**) CNS $CD45^{hi}CD3^{-}CD11c^{+}CD11b^{+}$ and $CD45^{hi}CD3^{-}CD11c^{+}CD11b^{-}$ cells were isolated from 10 normal mice, after which each DC subset (2×10^2 cells) was assessed in the DTH model in separate mice. Only $CD11b^{-}$ CNS DCs significantly reduced DTH to MOG ($n = 10$; $P = 0.011$; 3 independent experiments). (**E**) We repeated the experiment in **D**, except MOG was replaced by methylated BSA ($n = 3$/group). There was no significant modulation of methylated BSA response ($P > 0.9$), which — in contrast to MOG DTH DC–mediated modulation — suggests a CNS-antigen specific mechanism. Data represent mean ± SEM. $^{*}P < 0.05$.

tively, did not enhance neuroinflammation, failed to induce EAE, and/or did not mediate changes in DTH. This confirmed that in order for fingolimod to increase neuroinflammation, it is necessary to target the RMS specifically (Figures 5–7). While it is possible that antigen liberated by CNS trauma as a result of targeted fingolimod treatment might induce EAE, this seems unlikely. Control mice were treated similarly and did not get EAE, despite the release of potential antigens. Direct vaccination of 2D2 mice with MOG peptide without pertussis toxin also does not induce EAE (34). Furthermore, the available literature regarding fingolimod indicates that its direct action on the CNS and inflammatory cells, including Tregs, would reduce EAE severity and incidence (48). Finally, we showed that the effects of fingolimod on CNS DCs did not alter their regulation of inflammation in the models that we used, but directly affected their migration. Therefore, our present data indicate that pDCs associated with the RMS are targeted by fingolimod, preventing them from accessing the CxLNs. The resulting deficit led to changes in Treg function and induced Teff activation that caused exacerbation or induction of EAE.

DCs are also likely to have a role in the recently found benefit of alemtuzumab, a monoclonal therapeutic antibody currently in trials for the treatment of MS. Alemtuzumab promotes pDC dif-

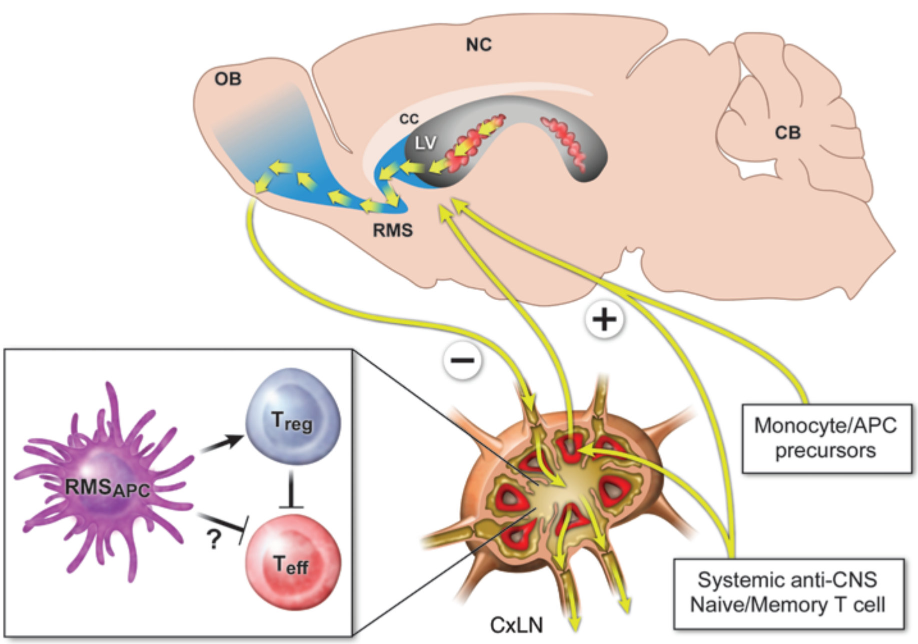

Figure 9
Immune cell migratory pathway through the RMS. Circulating DCs are recruited to the subventricular zone and RMS, most likely via the choroid plexus and/or associated vasculature. Migrating along the RMS toward the OB, these APCs encounter CNS antigens, perhaps from dying progenitors or neurons destined for replacement. DCs then exit the brain at the central terminus of RMS in the OB and access the CxLNs, where they regulate immunity. We suggest that they promote the differentiation and/or function of Tregs, which in turn suppress anti-CNS autoreactive naive cell or memory Teff responses in the CxLNs. Only previously activated Th cells are recruited to the CNS. NC, neural cortex; CB, cerebellum.

ferentiation and Treg expansion (15). pDCs are known to promote Treg expansion in animal models of MS (40). Further immune modification via alemtuzumab treatment appears to enhance protective anti-CNS autoimmunity in MS, producing brain-derived neurotrophic factor elaborating T cells in the periphery, an effect that is likely mediated by DCs. We also found that the subset of DCs that downregulated CNS immune responses in the CxLNs was also likely to contain pDCs, which are CD11c$^+$CD11b$^-$. Although our present studies were undertaken in mice, the CxLNs regulate immunity in human neuroinflammatory disease (13), and the RMS has also been anatomically defined in humans (49). Although there has been controversy regarding the neurogenic function of the RMS in adult humans (49–53), its role as a conduit for other cell types is yet to be explored, and the distribution of CNS parenchymal DCs in humans is reportedly similar to that seen in mice (5, 32).

Lastly, the RMS–immune cell migratory pathway is capable of being manipulated, as indicated by our delivery of syngeneic DCs to the CxLNs. This demonstrated the feasibility of delivering local therapeutics that ultimately influence immune function at the level of the CxLNs in order to treat neuroinflammatory disease. The major advantage of such localized approaches to therapy is that significantly lower doses of drug could be delivered to achieve high concentrations at key sites of action, while minimizing untoward, dose-related, systemic side effects. These data provide a potential mechanism by which fingolimod might cause an adverse outcome in MS, but first and foremost, they markedly revise our understanding of the pathways of immune cellular traffic through the CNS and the consequences of intercommunication between the immune and CNS compartments in the maintenance of CNS tissue homeostasis in health and disease.

Methods

All mice were on the C57BL/6 background. Female C57BL/6 mice, 6–12 weeks of age, were purchased from Australian BioResources. 2D2 transgenic mice were a gift from V. Kuchroo (Brigham and Women's Hospital, Boston, Massachusetts, USA; refs. 33, 34). In *Cx3cr1*$^{+/gfp}$ mice, the coding sequence for EGFP was inserted into the *Cx3cr1* coding region via targeted deletion, rendering the Cx$_3$CR1/fractalkine receptor nonfunctional, and placing EGFP under *Cx3cr1* promoter control in the mutant allele (25). Mice were housed in the Garvan Institute Biological Testing Facility (BTF) or Salk Institute animal facilities and maintained on a 12-hour light/12-hour dark cycle, with standard free chow and water freely available. EAE was induced and clinically monitored as previously described with MOG$_{35-55}$ (46). EAE was clinically scored using a standard 1–5 scale.

A 30-gauge infusion cannula (Alzet) was implanted in the right lateral ventricle (icv; +0.2 mm anteroposterior, +1.0 mm lateral, 2.2 mm depth or 0, +1.0 mm lateral, 2.2 mm depth), the rostral forebrain (RFB) parenchyma (+0.7 mm anteroposterior, +1.1 mm lateral, 2.2 mm depth), or the hippocampus (–2.5 mm anteroposterior, +1.0 mm lateral, 2.7 depth). A catheter tube was connected from the infusion cannula to an osmotic pump implanted s.c. Cannula placements were confirmed postmortem in sections stained for Nissl material (Figure 6A). For targeting of the CxLNs, an incision was made at the base of the skull, and the catheter tube was tunneled under the scalp, such that the tip was at the position of the bregma in the midline. The catheter tube was sutured into position, primed to ensure patency, and connected to the s.c. infusion pump.

Generation of BM chimeras. BM chimeras were generated as described previously (54). In brief, recipient WT mice aged 6 weeks were irradiated with 2 doses of 5.5 Gy, 14 hours apart. Donor *Cx3cr1*$^{+/gfp}$ mice were killed, and BM was harvested from the femora and tibiae. At 3 hours after the second dose of irradiation, recipient mice received an injection of 3–5 × 10^6 BM cells (in 150 μl RPMI) i.v. via the lateral tail vein.

Isolation of LN and CNS mononuclear cells. CNS and LNs were removed from saline-perfused mice and cut into 2-mm pieces prior to digestion with collagenase D (2.5 mg/ml) and DNase I (1 mg/ml) in R10 media (RPMI 1640 medium) supplemented with 10% (v/v) FCS, 2 mM L-glutamine, 100 U/ml penicillin, 100 μg/ml streptomycin, and 50 μM 2-mecaptoethanol for 45 minutes at 37°C. Tissues were then passed through a cell strainer, followed by a Percoll gradient (70%/37%) and 350 *g* centrifugation. Mononuclear cells were removed from the interphase, washed twice, and resuspended in R10 medium supplemented with 10% (v/v) FCS.

Immunohistochemistry (IHC). CNS tissue was examined by IHC and immunofluorescence (IF) as previously described (46). Briefly, mice were deeply anesthetized (1 ml/2 kg euthal, 17% pentobarbitone sodium, 2.5% phenytoin sodium) and perfused through the left ventricle with 10 ml 0.9% saline, followed by 150 ml ice-cold 4% paraformaldehyde in sodium borate buffer at pH 9.5 using a peristaltic pump (Gilson). Brains were harvested, postfixed in 4% paraformaldehyde for 5 hours, and cryoprotected for 16 hours in 20% sucrose/50 mM potassium PBS (KPBS) at 4°C. Next, 30-μm-thick frozen brain sections were obtained with a sliding microtome (SM2010R; Leica Biosystem). Sections were stored in cryoprotectant solution (30% ethylene glycol, 20% glycol in 50 mM sodium phosphate buffer, pH 7.4) at –20°C.

Dual immunolabeling was performed as detailed previously (46). Briefly, 30-μm-thick floating tissue sections were treated with 0.3% hydrogen peroxide for 10 minutes to inhibit endogenous peroxidase, followed by 7 minutes of 1% sodium borohydride. Tissue sections were then immunostained with monoclonal antibody against CD11c (Armenian hamster anti-mCD11c; 1:1,000; clone N418, eBioscience) or CD3 (anti-CD3; KT3; 1:1,000; Chemicon) in 2% goat or donkey serum and 0.3% Triton X-100. Tissue sections were incubated in primary antibody for 48 hours at 4°C on an orbital rocker (50 rpm; Ratek Instrument), followed by biotinylated secondary staining (goat or donkey; 1:200; Jackson Immunoresearch) in the same buffer as above for 1 hour at room temperature. After secondary immunostaining, sections were labeled with avidin using the Vecta Elite kit (Vector Laboratorie) per the manufacturer's protocol. After avidin labeling, sections were washed twice (10 minutes per wash) in 0.1 M sodium acetate, pH 6, followed by development in nickel-enhanced DAB (2.5% nickel ammonium sulfate, 100 mM sodium acetate, 0.5 mg/ml DAB, 2 mg/ml D β-glucose, 0.4 mg/ml ammonium chloride, 1 U/ml glucose oxidase; Sigma-Aldrich) for 5–7 minutes at 4°C for black-colored labeling. Sections were washed 3 times (10 minutes per wash) in KPBS and incubated with the second primary antibody against CD11c or DCX (sc-8066; Santacruz Biotech) overnight, under the same conditions as for the initial primary antibody, followed by the appropriate biotinylated-secondary staining (donkey; 1:200; Jackson Immunoresearch) and avidin labeling procedures. Sections were then washed twice (10 minutes per wash) with KPBS, and staining was developed in DAB without nickel enhancement (0.5 mg/ml DAB, 2 mg/ml D β-glucose, 0.4 mg/ml ammonium chloride, 1 U/ml glucose oxidase; Sigma-Aldrich) in KPBS to give brown labeling. Sections were mounted onto gelatin-coated slides, then dehydrated and coverslipped with DPX (Electron Microscopy Sciences). For combined immunoperoxidase and IF staining, sections were labeled with anti-CD11c and developed with nickel-enhanced DAB, followed by incubation with anti-DCX and with a species-specific FITC-labeled secondary antibody. Sections were mounted on gelatin-coated slides in an aqueous mounting buffer and coverslipped.

IF confocal microscopy. Sections were subjected to IF triple staining; guinea pig anti-DCX (1:2,000; Millipore), Armenian hamster anti-CD11c (1:800; eBioscience), and rat anti-CD11b (1:500; BD Biosciences) or rat anti-CD31 (1:100; BD Biosciences) were added in incubation buffer (0.1M PBS containing 0.3% Triton-X100 with both 2% normal donkey and 2% normal goat serum), and staining was done at 4°C for 24 hours. After washing with PBS 3 times, sections were then probed with fluorophore-labeled secondary antibodies (Jackson ImmunoResearch) at room temperature (RT) for 1 hour. The reaction was terminated by 3 washes in PBS, and sections were then mounted and coverslipped in 50% glycerol/PBS. Specimens from *Cx3cr1*$^{gfp/+}$-to-WT BM chimeric mice were treated similarly, except that double staining was performed instead. Brain sections from these mice were stained with DCX and CD11b or with CD11c and CD11b. Confocal images were obtained on a Leica TSC SP confocal microscope and processed using Adobe Photoshop CS2 v.9 software.

Cell quantification and mapping. To quantify and/or map DCs, we used dual-labeled IHC/IF material, as described above for CD11c with DCX (Figure 1). CD11c$^+$ cells associated with the RMS (DCX$^+$) were quantified in 6 separate SPF C57BL/6 mice, from its point of emergence at the level of the subventricular zone (in at least 5 sections per animal) to its entry to the OB. The corpus callosum and frontal cortex in the same sections were examined as white and gray matter controls, respectively. Cell counts were corrected using Abercrombie's method (55), and cell density was derived using the area examined (from Neurolucida reconstructions), defined as the DCX$^+$ area for the RMS or as the anatomical bounds of the corpus callosum and frontal cortex of the same sections.

Treatments. To demonstrate the migration of leukocytes through the RMS/CNS down to the CxLNs, mice were treated with vehicle (50% DMSO) or fingolimod (6 μg/d in 50% DMSO) i.p. for 8 days, commencing treatment 1 day prior to icv cannula placement and CFSE (1.2 mM in 50% DMSO) infusion for 7 days by s.c. osmotic minipump. Mononuclear cells from the brain, CxLNs, and ILNs were harvested while infusions were active. LN mononuclear cells were labeled with anti-CD45 (BD Biosciences — Pharmingen) alone and examined by FACS to show egress of CD45$^+$ cells from the CNS. CNS leukocytes were labeled with a cocktail of antibodies (all from BD Biosciences — Pharmingen), including anti-CD45 (PERCP rat anti-mouse CD45; 30-F11), anti-CD3 (pacific blue hamster anti-mouse CD3e; 500A2), anti-CD4 (Alexa Fluor 700 rat anti-mouse CD4; RM4-5), anti-CD11c (APC hamster anti-mouse CD11c; HL3), anti-CD11b (APC-Cy7 rat anti-mouse CD11b; M1/70), anti-B220 (PE rat anti-mouse CD45r/B220; RA3-6B2), and anti–mPDCA-1 (FITC rat anti-mouse PDCA-1; JF05-1C2.4.1) (Supplemental Figures 2 and 4).

To examine the effect of central fingolimod administration on EAE severity, C57BL/6 mice were cannulated for either icv or RFB (i.e., RMS-targeted) infusions, receiving 30 or 300 ng/d fingolimod or vehicle (50% DMSO) over 4 weeks. 1 week after initiating fingolimod infusion, EAE was induced as described above. 2D2 mice received RMS-fingolimod or RMS-vehicle (i.e., infusions of 300 ng/d fingolimod or vehicle through cannulae aimed at the RMS). As a control, fingolimod (300 ng/d) was targeted to the CxLNs (bypassing the CNS) by infusion under the scalp. Animals were examined for the development of clinical EAE. At the termination of the experiment, mice were perfused, and their brains and spinal cords were removed. After fixation, brains were sectioned and stained for Nissl material to evaluate cannula placements.

To examine the role of CXCR4 and CD73, AMD3100 (CXCR4 antagonist; MerckMillipore) and a CD73 antagonist (adenosine 5′-[α,β-methylene] diphosphate; ADP analog; Sigma-Aldrich) were used. ADP analog (0.5 mg in saline) was injected daily i.p. for 12 days. Mice were sacrificed while treatments were pharmacologically active, and mononuclear cells from the RFB denuded of meninges were isolated and examined by FACS (Supplemental Figures 2 and 4).

To ablate the RMS, ARA-c (Sigma-Aldrich), 2% in saline, was infused icv for 7 days by s.c. osmotic minipump. Mice were killed while the drug was active for CNS mononuclear cell analysis or IHC quantification of CD11c cells in the RMS.

Tracking transplanted DCs in the RMS in vivo. BM from C57BL/6 mice cultured in the presence of 300 ng/ml of recombinant murine Fms-like tyrosine kinase 3 ligand (FLT3) for 9 days. Successful DC maturation was confirmed by FACS analysis, which demonstrated that >95% of cells were CD45$^+$CD11c$^+$. Cells were labeled ex vivo in 2.6 μM CFSE for 5 minutes, washed, and then injected icv (1×10^6 cells). For ex vivo fingolimod treatment, cells were incubated in culture with 100 nM fingolimod for 24 hours prior to delivery. Animals were killed 16 and 24 hours after injection, and brains were processed as described above for IF staining for DCX or LN analysis at 48 hours.

Ex vivo Treg suppression cell assay. LNs from experimental mice, pretreated as described above, were harvested, and single-cell suspensions were obtained by passing the LN through a 70-μm nylon mesh in 1× PBS containing 5% FCS. Red blood cells were lysed on ice. To deplete Tregs from the cell suspension, cells were labeled with biotin–anti-CD25 beads (Miltenyi Biotec), or the same beads without antibody as a process control (per the manufacturer's instructions), and then passed through magnetic columns (Supplemental Figure 8). Cell suspensions with or without Tregs were incubated in the presence or absence of MOG$_{35-55}$ peptide (3 μg/ml) for 44 hours of stimulation. Cells were then washed 3 times with 1× PBS and labeled with fluorophore-conjugated antibodies to determine activated Teffs and Tregs using anti-CD3, -CD4, -Vβ11, -CD25, and CD69 followed by analysis (Supplemental Figure 9).

FACS analysis. Mononuclear cells were labeled and analyzed using a LSR II flow cytometric instrument (BD Biosciences). For determination of cell phenotypes isolated from the CNS, events were gated as shown in Supplemental Figures 2 and 4. To determine the proportion of antigen-specific T cells present in the spinal cord, Vβ11^{+}CD3^{+}CD4^{+} T cells were quantified using the gating strategy shown in Supplemental Figure 5. Brain mononuclear cell phenotyping was performed to determine the proportion of microglia (CD45^{int}), T cells (CD45^{hi}CD3^{+}CD4$^{+/-}$), DCs (CD45^{hi}CD3^{-}CD11c^{+}), macrophages/PMNs (CD45^{hi}CD3^{-}CD11c^{-}CD11b^{+}) and B cells (CD45^{hi}CD3^{-}CD11c^{-}CD11b^{-}B220^{+}; Supplemental Figure 4), and pDCs (CD45^{hi}CD3^{-}CD11c^{-}CD11b^{-}B220^{+}mPDCA-1^{+}; Supplemental Figures 2 and 4). In LNs from 2D2 mice, antigen-specific helper Teffs were defined as CD45^{+}CD44^{hi}CD62L^{-}CD3^{+}CD4^{+}Vβ11^{+}, and antigen-specific Tregs were defined as CD45^{+}Vβ11^{+}CD3^{+}CD4^{+}CD25^{hi}CD127^{lo} (Supplemental Figures 6 and 7 and ref. 56).

Isolation of CxLN DCs and DTH. The ability of DCs migrated from CNS to the CxLNs to mount an anti-MOG–specific immune response was investigated using a modified model of DTH (39). In brief, C57BL/6 mice were cannulated icv or via RFB to receive a continuous infusion of fingolimod (300 ng/d) or vehicle over 4 weeks. Animals were then killed and CxLNs removed; mononuclear cells were isolated as above while infusions were active. Cells were labeled with anti-CD3 and anti-CD11c antibodies. The CD3^{-}CD11c^{+} cell population was sorted to >99% purity using the Influx cell sorter (BD Biosciences) and the parameters shown in Supplemental Figure 9. The sorted cells (4–8 × 10^{4} cells/20 μl medium) were then injected into a pinna of a separate cohort of MOG-prevaccinated C57BL/6 mice (7 days before cell injection); the other pinna was injected with volume of acellular medium as a control. 10 days after injection, both pinnae were challenged with MOG peptide (50 μg/20 μl/ear). Ear thickness was measured before and 24 hours after MOG challenge using a digital micrometer. The DTH response was measured by subtracting the premanipulation ear thickness from the measurement 24 hours after challenge.

Statistics. As data were nonparametric, all comparisons were performed using the appropriate nonparametric test. Where serial measurements were taken over time, groups were compared using repeated-measures ANOVA. Regression analysis was performed using the method of Poisson. A P value less than 0.05 was considered significant, and reported values are 2-tailed where appropriate.

Study approval. The Animal Ethics Committees of the Garvan Institute or University of Queensland or the IACUC of the Salk Institute approved all work.

Acknowledgments

D.A. Brown is supported by Multiple Sclerosis Research Australia, The MS Angels Canberra, SpinalCure/NRMA, the National Multiple Sclerosis Society USA, Trish Multiple Sclerosis Research Foundation Australia, New South Wales Health Research and Development Infrastructure grants, and the NHMRC. P.E. Sawchenko is supported by NIH grant NS-21182, the Clayton Medical Research Foundation, and the Leona M. and Harry B. Helmsley Charitable Trust (no. 2012PG-MED002). D.A. Brown is a NHMRC Australia Biomedical Research Fellow and The Inaugural SpinalCure Australia Senior Research Fellow. M.J. Ruitenberg is supported by a SpinalCure Australia Career Development Fellowship. P.E. Sawchenko is a Senior Investigator of the Clayton Medical Research Foundation. The authors thank William Sewell for insightful review and helpful criticism of the manuscript during preparation.

Received for publication June 13, 2013, and accepted in revised form November 21, 2013.

Address correspondence to: David A. Brown, Laboratory of Neuroinflammation, St. Vincent's Centre for Applied Medical Research, 405 Liverpool St., Sydney 2010, New South Wales, Australia. Phone: 61.02.8382.4952; Fax: 61.02.8382.4971; E-mail: D.Brown@amr.org.au.

1. Murphy JB, Sturm E. Conditions determining the transplantability of tissues in the brain. *J Exp Med*. 1923;38(2):183–197.
2. Goverman J. Autoimmune T cell responses in the central nervous system. *Nat Rev Immunol*. 2009;9(6):393–407.
3. Kivisäkk P, et al. Localizing central nervous system immune surveillance: meningeal antigen-presenting cells activate T cells during experimental autoimmune encephalomyelitis. *Ann Neurol*. 2009;65(4):457–469.
4. Kebir H, et al. Human TH17 lymphocytes promote blood-brain barrier disruption and central nervous system inflammation. *Nat Med*. 2007;13(10):1173–1175.
5. Prodinger C, et al. CD11c-expressing cells reside in the juxtavascular parenchyma and extend processes into the glia limitans of the mouse nervous system. *Acta Neuropathol*. 2011;121(4):445–458.
6. Greter M, et al. Dendritic cells permit immune invasion of the CNS in an animal model of multiple sclerosis. *Nat Med*. 2005;11(3):328–334.
7. Ling C, Sandor M, Fabry Z. In situ processing and distribution of intracerebrally injected OVA in the CNS. *J Neuroimmunol*. 2003;141(1–2):90–98.
8. Karman J, Ling C, Sandor M, Fabry Z. Initiation of immune responses in brain is promoted by local dendritic cells. *J Immunol*. 2004;173(4):2353–2361.
9. Karman J, Chu HH, Co DO, Seroogy CM, Sandor M, Fabry Z. Dendritic cells amplify T cell-mediated immune responses in the central nervous system. *J Immunol*. 2006;177(11):7750–7760.
10. Serrats J, Schiltz JC, García-Bueno B, van Rooijen N, Reyes TM, Sawchenko PE. Dual roles for perivascular macrophages in immune-to-brain signaling. *Neuron*. 2010;65(1):94–106.
11. Lehner T. Special regulatory T cell review: The resurgence of the concept of contrasuppression in immunoregulation. *Immunology*. 2008;123(1):40–44.
12. Nemeth E, Baird AW, O'Farrelly C. Microanatomy of the liver immune system. *Semin Immunopathol*. 2009;31(3):333–343.
13. van Zwam M, et al. Brain antigens in functionally distinct antigen-presenting cell populations in cervical lymph nodes in MS and EAE. *J Mol Med*. 2009;87(3):273–286.
14. Ling C, Sandor M, Suresh M, Fabry Z. Traumatic injury and the presence of antigen differentially contribute to T-cell recruitment in the CNS. *J Neurosci*. 2006;26(3):731–741.
15. Jones JL, et al. Improvement in disability after alemtuzumab treatment of multiple sclerosis is associated with neuroprotective autoimmunity. *Brain*. 2010;133(pt 8):2232–2247.
16. Moalem G, Leibowitz-Amit R, Yoles E, Mor F, Cohen IR, Schwartz M. Autoimmune T cells protect neurons from secondary degeneration after central nervous system axotomy. *Nat Med*. 1999;5(1):49–55.
17. Schwartz M, Shechter R. Systemic inflammatory cells fight off neurodegenerative disease. *Nat Rev Neurol*. 2010;6(7):405–410.
18. Chun J, Hartung HP. Mechanism of action of oral fingolimod (FTY720) in multiple sclerosis. *Clin Neuropharmacol*. 2010;33(2):91–101.
19. Idzko M, et al. Local application of FTY720 to the lung abrogates experimental asthma by altering dendritic cell function. *J Clin Invest*. 2006;116(11):2935–2944.
20. Reines I, et al. Topical application of sphingosine-1-phosphate and FTY720 attenuate allergic contact dermatitis reaction through inhibition of dendritic cell migration. *J Invest Dermatol*. 2009;129(8):1954–1962.
21. Sawicka E, et al. The sphingosine 1-phosphate receptor agonist FTY720 differentially affects the sequestration of CD4+/CD25+ T-regulatory cells

and enhances their functional activity. *J Immunol*. 2005;175(12):7973–7980.

22. Pashenkov M, Teleshova N, Link H. Inflammation in the central nervous system: the role for dendritic cells. *Brain Pathol*. 2003;13(1):23–33.
23. Bulloch K, et al. CD11c/EYFP transgene illuminates a discrete network of dendritic cells within the embryonic, neonatal, adult, and injured mouse brain. *J Comp Neurol*. 2008;508(5):687–710.
24. Ransohoff RM, Perry VH. Microglial physiology: unique stimuli, specialized responses. *Annu Rev Immunol*. 2009;27:119–145.
25. Jung S, et al. Analysis of fractalkine receptor CX(3)CR1 function by targeted deletion and green fluorescent protein reporter gene insertion. *Mol Cell Biol*. 2000;20(11):4106–4114.
26. Shechter R, et al. Recruitment of beneficial M2 macrophages to injured spinal cord is orchestrated by remote brain choroid plexus. *Immunity*. 2013; 38(3):555–569.
27. Durafourt BA, Lambert C, Johnson TA, Blain M, Bar-Or A, Antel JP. Differential responses of human microglia and blood-derived myeloid cells to FTY720. *J Neuroimmunol*. 2011;230(1–2):10–16.
28. Naik SH, et al. Cutting edge: generation of splenic CD8+ and CD8- dendritic cell equivalents in Fms-like tyrosine kinase 3 ligand bone marrow cultures. *J Immunol*. 2005;174(11):6592–6597.
29. Nam SC, et al. Dynamic features of postnatal subventricular zone cell motility: a two-photon time-lapse study. *J Comp Neurol*. 2007;505(2):190–208.
30. Doetsch F, Garcia-Verdugo JM, Alvarez-Buylla A. Regeneration of a germinal layer in the adult mammalian brain. *Proc Natl Acad Sci U S A*. 1999;96(20):11619–11624.
31. Tran PB, Ren D, Veldhouse TJ, Miller RJ. Chemokine receptors are expressed widely by embryonic and adult neural progenitor cells. *J Neurosci Res*. 2004;76(1):20–34.
32. Foster CA, et al. Brain penetration of the oral immunomodulatory drug FTY720 and its phosphorylation in the central nervous system during experimental autoimmune encephalomyelitis: consequences for mode of action in multiple sclerosis. *J Pharmacol Exp Ther*. 2007;323(2):469–475.
33. Bettelli E, Baeten D, Jäger A, Sobel RA, Kuchroo VK. Myelin oligodendrocyte glycoprotein-specific T and B cells cooperate to induce a Devic-like disease in mice. *J Clin Invest*. 2006;116(9):2393–2402.
34. Bettelli E, Pagany M, Weiner HL, Linington C, Sobel RA, Kuchroo VK. Myelin oligodendrocyte glycoprotein-specific T cell receptor transgenic mice develop spontaneous autoimmune optic neuritis. *J Exp Med*. 2003;197(9):1073–1081.
35. Yadav R, Bhowmick S, Gorecki P, O'Rourke J, Cone RE. Paradoxical effect of pertussis toxin on the delayed hypersensitivity response to autoantigens in mice. *PLoS One*. 2010;5(8):e11983.
36. Hama Y, Koyama Y, Urano Y, Choyke PL, Kobayashi H. Two-color lymphatic mapping using Ig-conjugated near infrared optical probes. *J Invest Dermatol*. 2007;127(10):2351–2356.
37. Chen X, Fang L, Song S, Guo TB, Liu A, Zhang JZ. Thymic regulation of autoimmune disease by accelerated differentiation of Foxp3+ regulatory T cells through IL-7 signaling pathway. *J Immunol*. 2009; 183(10):6135–6144.
38. Bluestone JA, Abbas AK. Natural versus adaptive regulatory T cells. *Nat Rev Immunol*. 2003; 3(3):253–257.
39. Ng RL, Bisley JL, Gorman S, Norval M, Hart PH. Ultraviolet irradiation of mice reduces the competency of bone marrow-derived CD11c+ cells via an indomethacin-inhibitable pathway. *J Immunol*. 2010;185(12):7207–7215.
40. Bailey-Bucktrout SL, Caulkins SC, Goings G, Fischer JA, Dzionek A, Miller SD. Cutting edge: central nervous system plasmacytoid dendritic cells regulate the severity of relapsing experimental autoimmune encephalomyelitis. *J Immunol*. 2008;180(10):6457–6461.
41. Gottfried-Blackmore A, Kaunzner UW, Idoyaga J, Felger JC, McEwen BS, Bulloch K. Acute in vivo exposure to interferon-{gamma} enables resident brain dendritic cells to become effective antigen presenting cells. *Proc Natl Acad Sci U S A*. 2009;106 (49):20918–20923.
42. Weller RO, Engelhardt B, Phillips MJ. Lymphocyte targeting of the central nervous system: a review of afferent and efferent CNS-immune pathways. *Brain Pathol*. 1996;6(3):275–288.
43. Weller RO, Galea I, Carare RO, Minagar A. Pathophysiology of the lymphatic drainage of the central nervous system: Implications for pathogenesis and therapy of multiple sclerosis. *Pathophysiology*. 2009;system(4):295–306.
44. Ransohoff RM, Engelhardt B. The anatomical and cellular basis of immune surveillance in the central nervous system. *Nat Rev Immunol*. 2012; 12(9):623–635.
45. Daelman L, Maitrot A, Maarouf A, Chaunu MP, Papeix C, Tourbah A. Severe multiple sclerosis reactivation under fingolimod 3 months after natalizumab withdrawal. *Mult Scler*. 2012; 18(11):1647–1649.
46. Brown DA, Sawchenko PE. Time course and distribution of inflammatory and neurodegenerative events suggest structural bases for the pathogenesis of experimental autoimmune encephalomyelitis. *J Comp Neurol*. 2007;502(2):236–260.
47. McMahon EJ, Bailey SL, Castenada CV, Waldner H, Miller SD. Epitope spreading initiates in the CNS in two mouse models of multiple sclerosis. *Nat Med*. 2005;11(3):335–339.
48. Brinkmann V, et al. Fingolimod (FTY720): discovery and development of an oral drug to treat multiple sclerosis. *Nat Rev Drug Discov*. 2010; 9(11):883–897.
49. Curtis MA, et al. Human neuroblasts migrate to the olfactory bulb via a lateral ventricular extension. *Science*. 2007;315(5816):1243–1249.
50. Sanai N, et al. Corridors of migrating neurons in the human brain and their decline during infancy. *Nature*. 2011;478(7369):382–386.
51. Scranton RA, Fletcher L, Sprague S, Jimenez DF, Digicaylioglu M. The rostral migratory stream plays a key role in intranasal delivery of drugs into the CNS. *PLoS One*. 2011;6(4):e18711.
52. Wang C, et al. Identification and characterization of neuroblasts in the subventricular zone and rostral migratory stream of the adult human brain. *Cell Res*. 2011;21(11):1534–1550.
53. Yang Z, Ming GL, Song H. Postnatal neurogenesis in the human forebrain: from two migratory streams to dribbles. *Cell Stem Cell*. 2011; 9(5):385–386.
54. Chinnery HR, Ruitenberg MJ, McMenamin PG. Novel characterization of monocyte-derived cell populations in the meninges and choroid plexus and their rates of replenishment in bone marrow chimeric mice. *J Neuropathol Exp Neurol*. 2010; 69(9):896–909.
55. Abercrombie M, Johnson ML. Quantitative histology of Wallerian degeneration: I. Nuclear population in rabbit sciatic nerve. *J Anat*. 1946; 80(pt 1):37–50.
56. Seddiki N, et al. Expression of interleukin (IL)-2 and IL-7 receptors discriminates between human regulatory and activated T cells. *J Exp Med*. 2006; 203(7):1693–1700.